Polarforschung 85 (2), 89–99, 2015 (erschienen 2016)

Sensitivity of Grounding-Line Dynamics to Viscoelastic Deformation of the Solid-Earth in an Idealized Scenario

by Hannes Konrad[1*], Ingo Sasgen[1], Volker Klemann[1], Malte Thoma[2], Klaus Grosfeld[2] and Zdeněk Martinec[3, 4]

Abstract: We investigate the behaviour of the grounding line (GL) of an idealised ice sheet and ice shelf by coupling a thermomechanical ice-sheet model to a self-gravitating viscoelastic solid-Earth model (SGVEM) in which a gravitationally self-consistent sea-level evolution is considered. The steady-state ice-sheet – shelf configuration is subject to forcing by sea-level rise, or altered surface mass balance and basal conditions, resulting in a retreat of the GL. We confirm previous studies showing that GL retreat can be decelerated and stopped by viscoelastic deformation of the solid Earth. We focus on the influence of lithosphere thickness and the upper mantle viscosity on the GL retreat and find that the time scales of solid-Earth relaxation, which are parameterised by the upper mantle viscosity, are most important for GL stability. We compare these retreat characteristics with results from the simpler "elastic lithosphere – relaxing asthenosphere" (ELRA) approximation of solid-Earth deformation, which is common in ice-sheet modelling. We find that the inconsistent description of sea level and the simplified relaxation behaviour of the ELRA approximation introduce an artificial bias on GL migration. Finally, we discuss the implications of similar time scales, on which ice dynamics and solid-Earth adjustment proceed, for the long-term stability of the ice sheet.

Zusammenfassung: Wir untersuchen das Verhalten der Aufsetzlinie eines idealisierten Eisschildes mit angrenzendem Schelfeis, indem wir ein numerisches thermomechanisches Eisschildmodell mit einem selbstgravitativen, viskoelastischen Modell für die feste Erde koppeln. In letzterem werden Meeresspiegeländerungen gravitativ konsistent berücksichtigt. Das gegebene Gleichgewicht, in welchem sich das System aus Eisschild und -schelf befindet, wird durch Anstieg des Meeresspiegels, bzw. veränderte Oberflächenmassenbilanz und basale Randbedingungen gestört, wodurch sich die Aufsetzlinie zurückzieht. Wie bereits in früheren Studien beschrieben, kann die viskoelastische Deformation der festen Erde den Rückzug der Aufsetzlinie bremsen und stoppen. Ein besonderes Augenmerk wird darauf gerichtet, wie sich der Einfluss der Lithosphärenmächtigkeit sowie der Viskosität des oberen Mantels auf den Rückzug der Aufsetzlinie auswirkt. Dabei stellen sich die Relaxationszeiten der festen Erde, die durch die Viskosität des oberen Mantels gegeben sind, als wichtigste Parameter für die Stabilität der Aufsetzlinie heraus. Die damit einhergehenden Rückzugsmerkmale werden mit Ergebnissen verglichen, die durch Anwendung einer vereinfachten Berücksichtigung der festen Erde („elastische Lithosphäre – relaxierende Asthenosphäre", ELRA) erzielt werden, wie es in der Modellierung von Eisschilden üblich ist. Wir zeigen, dass die inkonsistente Beschreibung des Meeresspiegels, sowie das vereinfachte Relaxationsverhalten der festen Erde die Bewegung der Aufsetzlinie beeinflussen. Schließlich behandeln wir die Implikationen ähnlicher Zeitskalen von Eis- und Erddynamik auf die langfristige Stabilität eines Eisschildes.

doi:10.2312/polfor.2016.005

[1] Helmholtz Centre Potsdam, German Research Centre for Geosciences GFZ, Telegrafenberg, 14473 Potsdam, Germany;
[*] now at School of Earth and Environment, University of Leeds, Leeds LS2 9JT, United Kingdom, <h.h.konrad@leeds.ac.uk>
[2] Alfred Wegener Institute, Helmholtz Centre for Polar and Marine Research, Am Handelshafen 12, 27570 Bremerhaven, Germany.
[3] Dublin Institute of Advanced Studies, 5 Merrion Square, Dublin 2, Ireland.
[4] Department of Geophysics, Charles University, V Holešovičkách 2, 18000 Praha 8, Czech Republic.
This paper was presented as a poster contribution at the International Conference "Our Climate – Our Future: Regional Perspectives on a Global Challenge", 6–9 October 2014 in Berlin, Germany.
Manuscript received 27 May 2015; revised version 09 December 2015; accepted 28 December 2015.

INTRODUCTION

The advance and retreat of the large continental ice sheets during glacial cycles load and unload the solid-Earth and thereby force viscoelastic deformation in the Earth's interior (Peltier 1974). In the ice sheet's vicinity, the deformation leads to subsidence of the Earth's surface in response to ice advance (loading) and uplift in response to retreat (unloading). Both are delayed by decades to millennia through the viscous flow in the Earth's mantle (Haskell 1935). The redistribution of ice masses, ocean masses due to ice discharge into the oceans and mantle material also induce changes in the gravity field, which affects the sea level as this coincides with the geoid, an equipotential surface of the gravity field.

The ice sheet's dynamical evolution is influenced by the Earth's response, mainly via three feedback mechanisms. First, a vertically moving ice – bedrock interface implies respective vertical motion of the ice-sheet surface. The uplift or subsidence of the ice – atmosphere interface leads to less or more ice accumulation in the interior accumulation areas (Oerlemans 1980, Huybrechts 1993). Second, the slopes of the bedrock topography, which are important boundary conditions for the near-bed ice velocities, are tilted by the vertical motion of the Earth's surface. Third, the ocean depth (or relative sea level RSL (all acronyms and labels are listed in Tab. 1) at the grounding line (GL, the transition from the ice sheet to the adjacent ice shelves), and thereby the GL positioning itself, is determined by the solid-Earth gravitational response and vertical motion of the ocean bottom. Accounting for this feedback in numerical ice-sheet models is of great importance, as glacial/interglacial sea-level variations are a major driver of ice-sheet advance and retreat (e.g., Pollard & DeConto 2009).

In our study, we employ a coupled numerical model for ice and solid-Earth dynamics, the latter one featuring a gravitationally consistent description of sea level. With the first two feedbacks treated by Konrad et al. (2014), this study addresses the feedback between RSL and GL dynamics, particularly in the case of an ice sheet subject to the Marine Ice Sheet Instability (MISI). Such an ice sheet is characterized by marine-based portions on bedrock, which deepens inland from the GL, as it is the case for the West Antarctic Ice Sheet. As the GL retreats downslope, the outflow across the GL into the ice shelf increases as the RSL increases due to the deepening. This leads to on-going disintegration of the ice sheet (Thomas & Bentley 1978, Schoof 2007).

Gomez et al. (2012) found in idealised numerical simulations that such an ice sheet can be stabilised by viscoelastic uplift following the unloading of the solid Earth by GL retreat.

Acronym A	Label L	Meaning
ACCU	L	Forcing scenario based on SMB reduction
BASL	L	Forcing scenario based on SMB and basal friction reduction
ERLA	A	Elastic Lithosphere / Relaxing Asthenosphere
ESL	A	Equivalent Sea Level
GL	A	Grounding Line
GMT	A	Generic Mapping Tool
ISM	A	Ice Sheet Model
MISI	A	Marine Ice Sheet Instability
PREM	A	Preliminary Earth Reference Model
RIGID	L	Viscoelastic layering in VILMA
RIMBAY	A	Revised Ice Sheet Model Based on frAnk pattYn (employed ice sheet model)
RSL	A	Relative Sea Level
S120	L	Forcing scenario based on sea-level rise
S150	L	Forcing scenario based on sea-level rise
SGVEM	A	Self-Gravitating ViscoElastic Earth Model
SIA	A	Shallow Ice Approximation
SLE	A	Sea Level Equation
SMB	A	Surface Mass Balance
SSA	A	Shallow Shelf Approximation
VE_L035_M19	L	viscoelastic layering in VILMA
VE_L100_M19	L	viscoelastic layering in VILMA
VE_L035_M21	L	viscoelastic layering in VILMA
VE_L100_M21	L	viscoelastic layering in VILMA
VILMA	A	Viscoelastic Lithosphere and MAntle model (employed Earth model)

Tab. 1: List of all used acronyms (A) and labels (L).

Tab. 1: Liste aller verwendeten Akronyme (A) und Bezeichnungen (L).

Similar to this study, we extensively analyse the influence of the Earth-model parameters on the ice-sheet – shelf dynamics. In a geometrically simplified ice-sheet scenario, the sensitivity of the GL position to the viscoelastic structure of the underlying solid Earth is investigated, in particular to the thickness of the lithosphere and to upper-mantle viscosity. Starting from an ice-sheet and ice-shelf configuration in steady state, the coupled model system is subject to a forcing by sea-level rise from ice melting on a remote continent – similar to the Antarctic Ice Sheet under the influence of Northern Hemispheric melt-water pulses during the deglaciation after the Last Glacial Maximum – as well as to changes in the boundary conditions at the ice-sheet surface and at the ice-sheet – bedrock interface.

Additionally, we employ the common approximate approach to solid-Earth dynamics in ice-sheet modelling, the so-called "elastic lithosphere – relaxing asthenosphere" (ELRA) approximation (e.g., Le Meur & Huybrechts 1996). Here, the lithosphere is considered as a thin and horizontally infinitely extended plate, whereas the viscous mantle flow is approximated by one *a priori* relaxation time. Sea level cannot be treated gravitationally consistently in ELRA. Consequently, eustatic sea-level variations are prescribed in the ice-sheet model (ISM) domain.

MODELLING

Ice-sheet modelling

We employ the thermomechanical ISM RIMBAY (Thoma et al. 2014). In the applied configuration, it solves for ice thickness, ice temperature and ice velocity by applying the Shallow Ice Approximation (SIA) for the linear momentum balance for grounded ice and the Shallow Shelf Approximation (SSA) for floating ice. In a transition zone, the solutions from SIA and SSA are mixed (e.g., Thoma et al. (2014) for details). The ISM domain is resolved with a 10 × 10 km Cartesian grid.

A constant rate factor A as well as the common value of $n = 3$ for the flow law exponent in Glen's Flow law for the viscous deformation of polycrystalline ice (Cuffey & Paterson 2010) is applied. A power law for basal sliding (Weertman 1957) is employed, parameterised by the basal sliding coefficient C and the basal sliding exponent $m = 1/3$ (Thoma et al. 2014).

The applied parameterisation for basal melt rates in the floating areas ($\dot{b}_B^{shelf}$) follows Beckmann & Goosse (2003):

$$\dot{b}_B^{shelf} = A_{eff} \frac{\rho_{oc}\, c_{p,oc}}{\rho L_{Ice}} \gamma_T (T_{oc} - T_{fp}) \quad (1)$$

where the freezing-point temperature at the ice-shelf base T_{fp} is computed as (Foldvik & Kvinge 1974)

$$T_{fp} = 0.0939°C - 0.057°C\,(PSU)^{-1}\, S_{oc} - 7.64 \bullet 10^{-4}°C\, m^{-1}\, z_{bsl} \quad (2)$$

Here, z_{bsl} is the depth below sea level of the ice-shelf base. The tuning parameter A_{eff} in Equation 1 specifies the "effective melting area". The remaining quantities in equations 1 and 2 are the ocean water density $\varrho_{oc} = 1028$ kg m^{-3}, the specific heat of ocean water $c_{p,oc} = 3974$ J (kg °C)$^{-1}$, the latent heat of the ice – water transition $L_{Ice} = 333.5$ kJ kg^{-1}, the ocean temperature $T_{oc} = -1.7$ °C, the salinity $S_{oc} = 35$ PSU, and the exchange velocity $\gamma_T = 10^{-4}$ m/s.

In the applied configuration, the calving front, where the ice shelves do not only share a vertical boundary with the ocean, but also a horizontal one, can only retreat but not advance in the model. Retreat occurs if the ice thickness at the calving front goes down to zero. Advance is not modelled explicitly here. Instead, all ice that is flowing accross the front is assumed to have calved off and by that has gone into the ocean.

Solid-Earth and sea-level model

We employ the self-gravitating viscoelastic Earth model (SGVEM) developed by Martinec (2000) in the implementation VILMA. Under the assumption of a spherical and incompressible Earth in hydrostatic equilibrium at the initial time, the equations for mass continuity and linearised linear momentum balance, the Poisson equation for the incremental gravitational potential and the constitutive equation of a Maxwell viscoelastic solid are solved. The SGVEM is composed of a fluid core, a viscoelastically stratified mantle and an elastic lithosphere. With the angular dependencies treated by spherical harmonics and the radial dependencies by

finite-elements, the model approach is referred to as a spectral-finite-elements approach. The Legendre cut-off degree has been fixed to $j = 256$ (KONRAD et al. 2014) (~80 km spatial resolution).

The sea-level equation (SLE, FARRELL & CLARK 1976, MITROVICA & MILNE 2003) has been implemented by HAGEDOORN et al. (2007). Based on the surface load σ as the forcing quantity of viscoelastic deformation in the solid-Earth, it solves for changes of RSL Δs_{rsl} by ensuring (1) the coincidence of the ocean surface with an equipotential surface of the gravity field and (2) the conservation of the global water budget during the exchange of water masses between ice sheets and oceans. Changes in the rotational potential due to the redistribution of surface masses are also taken into account. The surface load σ is given by changes in the weight of the ice or ocean column, depending on whether a specific location is covered by grounded ice or flooded with ocean water. In the case of a migrating GL, the vanishing weight of the initial ice or ocean-water column at a location traversed by the GL is partially compensated by inflowing ocean water or an advancing ice sheet, respectively, which is corrected for in the surface load.

An important feature of the modelled sea-level variations in response to the redistribution of ice and ocean masses and mantle material is their non-uniformity (MITROVICA et al. 2001, SPADA et al. 2013). Especially in the vicinity of advancing or retreating ice sheets, the sea level deviates strongly from the global mean.

ELRA

In ice-sheet modelling, the ELRA approximation of solid-Earth relaxation is often applied (e.g., HUYBRECHTS et al. 2011, GREVE et al. 2011, POLLARD & DECONTO 2012, BINDSCHADLER et al. 2013, MARIS et al. 2014). It is based on two assumptions. First, the lithosphere is considered as a thin plate characterised by its flexural rigidity D (in N m). Following BROTCHIE & SILVESTER (1969) and LE MEUR & HUYBRECHTS (1996), its equilibrium deflectional response to a surface load σ as a function of horizontal coordinates x and y can be written as

$$U_{eq}(x,y,t) = \frac{gL_r^2}{2\pi D}\int \sigma(x',y',t) \bullet \chi\left(\sqrt{(x-x')^2+(y-y')^2}/\,L_r\right)dx'dy' \quad (3)$$

Here, $g = 9.81$ m s^{-2} is the gravitational acceleration at the Earth's surface, $L_r = (D/\varrho_a/g)^{0.25}$ is the radius of relative stiffness with $\varrho_a = 3300$ kg m^{-3} being the asthenosphere density, and χ is the Kelvin function of zeroth order (e.g., ABRAMOWITZ & STEGUN 1964).

Second, the viscous mantle flow is modelled by one *a priori* relaxation time τ_r, so that the actual lithospheric deflection U is given by

$$\frac{\partial U}{\partial t} = -\frac{U-U_{eq}}{\tau_r} \quad (4)$$

The gravitationally consistent non-uniform sea-level variations as described for the SGVEM in Section 2.2, cannot be solved for in the ELRA approximation. Instead, eustatic (i.e., global average) sea-level variations are applied here, by which the local sealevel is typically overestimated (e.g., GOMEZ et al. 2013).

Coupling

In contrast to other comparable model systems (LE MEUR & HUYBRECHTS 1996, VAN DEN BERG et al. 2008, GOMEZ et al. 2012, 2013, DE BOER et al. 2014), the coupling of the ISM and the SGVEM employed in this study is straightforward: The weak formulation of the solid-Earth dynamics (MARTINEC 2000) – in contrast to the normal-mode approach (PELTIER 1974) used by the Earth models employed in the above coupling studies – allows an explicit time stepping, so that the two models can run synchronously in time. The ISM runs from one coupling time step t_i to the next $t_{i+1} = t_i + \Delta t_c$ while linearly extrapolating the sea-level and the bedrock-deformation fields from the last two coupling time steps (t_i, t_{i-1}) in time. Then, ice thickness changes are handed to the SGVEM, which now also runs from t_i to t_{i+1} while linearly interpolating ice thickness in time. After handing sea level and bedrock deformation at t_{i+1} from the SGVEM to the ISM, the coupling procedure is finished for the interval from t_i to t_{i+1}. The explicit time stepping also allows a much shorter coupling interval (here, Δt_c = 50 yr) than most of the above studies.

The ISM operates on a regional equidistant Cartesian grid, whereas the SLE in the SGVEM is solved on a global Gauss-Legendre grid for geographical latitude (512 nodes) and longitude (1024 nodes). Hence, the exchanged fields need to be regridded. We opt for centering the ISM model domain at the equator, so that the Gauss-Legendre grid is almost equidistant in the x and y coordinates of the ISM grid (~39 km, four times the horizontal ISM resolution). This would not be the case if the ISM domain was centered at a pole. Our choice makes Delaunay triangulation as provided by the Generic Mapping Tool (GMT, WESSEL & SMITH 1991) a suitable choice for regridding the ice-thickness changes to the global grid. The sea-level and bedrock-deformation fields are regridded by bicubic interpolation to the regional Cartesian grid, again using GMT (e.g., KONRAD et al. 2014). Please note that this choice for an equatorial situation of the ice sheet is only due to the relation of the two numerical models' grids and has no implications for the climatic forcing of the ice sheet, as the latter is prescribed separately and independently from the location of the ice sheet, see below.

SCENARIO

Steady-state ice sheet

The steady-state set-up at the beginning of the perturbation experiments ($t = 0$) comprises an ice shelf which is confined at three sides by an ice sheet (Fig. 1A, B, C). This ice-sheet geometry is reached after 60 kyr of initialization (i.e., starting at t = -60 kyr) under a constant surface mass balance (SMB) of 0.2 m/yr, a surface temperature of -15 °C, and a basal sliding coefficient of $C = 10^7$ Pa (m/s)$^{1/3}$. The melting rates in the ice shelf areas are forced to be close to zero compared to the accumulation rate by setting the adjustment parameter in Equation 1 to $A_{eff} = 0.001$ m^2. The bedrock topography is designed

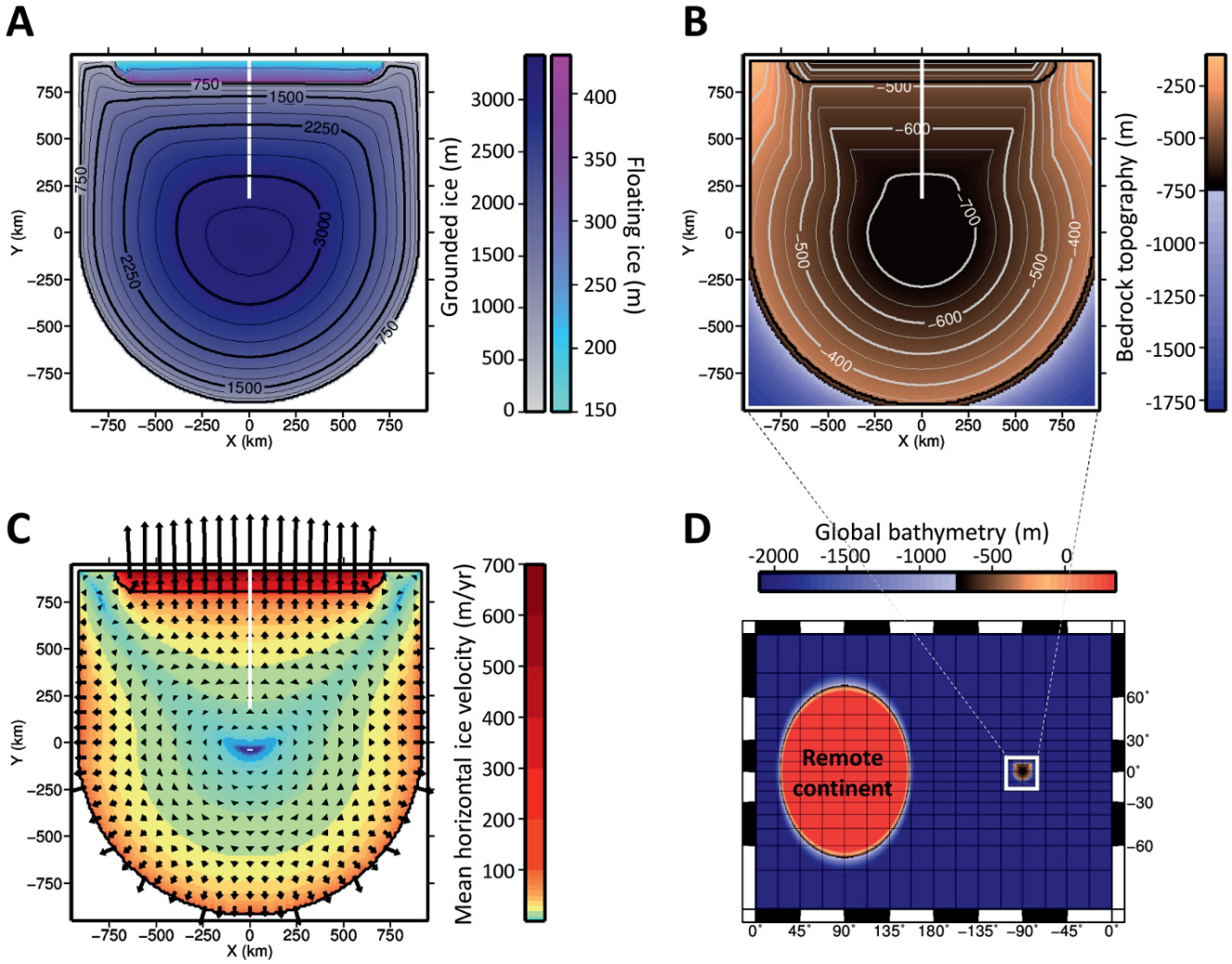

Fig. 1: Initial set-up of the considered model configuration. A: Ice thickness; note the different colour scales for grounded and floating ice. B: Bedrock topography; the topography is referenced to sea level at $t = 0$. C: Mean horizontal ice velocities; in B and C, the black lines mark the transition between grounded ice, floating ice, and ocean. The white line at $x = 0$ indicates the cross section along which the results are analysed. D: Global bathymetry featuring the ISM domain (-90° longitude), a remote circular continent (+90° longitude; in Mercator projection appearing as elliptical), and an ocean.

Abb. 1: Zustand des Modellsystems zu Beginn des Experiments. A: Eismächtigkeit; beachte die unterschiedlichen Farbskalen für aufsitzendes und aufschwimmendes Eis. B: Topographie des Felsbettes, bezogen auf den Meeresspiegel zum Zeitpunkt $t = 0$. C: Mittlere horizontale Geschwindigkeiten des Eises. Die schwarzen Linien in B und C stellen die Übergänge zwischen aufsitzendem und aufschwimmendem Eis, sowie dem Ozean dar. Die weiße Linie bei $x = 0$ zeigt den Querschnitt an, entlang dessen die Ergebnisse betrachtet werden. D: Globale Bathymetrie, bestehend aus dem Eismodellbereich (bei -90° geografischer Länge), einem entfernt davon liegenden kreisförmigen Kontinent (bei +90° geografischer Länge; erscheint in der Mercator-Projektion elliptisch) und einem Ozean.

symmetrically with respect to the y-axis and features an inland slope such that a GL perturbation will cause further retreat (MISI; see "Introduction"). The solid-Earth is in rest at $t = 0$ (hydrostatic equilibrium).

Global bathymetry

The SGVEM requires a global bathymetry ζ (Ω,$t = 0$) for initialization. The applied bathymetry (Fig. 1D) incorporates the ISM domain continent at the Equator with the y-axis of the ISM domain, coinciding with the meridian at ϕ = -90° (270°) longitude (positive y-axis points to the North Pole; positive x-axis points eastward). A remote continent (circular with radius r_{cont} = 7000 km and altitude ζ_{cont} = 300 m above sea-level) is equatorially centered as an antipode to this continent at ϕ = +90°. The remaining part of the planet is deep ocean (ζ_{ocean} = -2000 m) and distance-weighted interpolations between continental altitudes and deep ocean depth in transition zones around the two continents.

Solid-Earth representation

The Earth structure is given by radially symmetric (i.e., one-dimensional) distributions of viscosity and shear modulus. In this study, five different sets of solid-Earth parameters are applied (Tab. 2). Four of them are three-layered, obtained by combining a thin or a thick lithosphere (h_L = 35 km vs. 100 km) with a low-viscous or a high-viscous upper mantle (η_{UM} = 1×10^{19} Pa s *versus* 1×10^{21} Pa s). In these cases, the lower mantle has a viscosity of η_{LM} = 1×10^{22} Pa s. The boundary between upper and lower mantle is at 670 km depth. The core-mantle boundary is at 2891 km depth. The shear modulus in these settings is adopted from the Preliminary Earth Reference Model (PREM, Dziewonski & Anderson 1981).

Label	h_L (km)	η_{UM} (P as)	η_{LM} (P as)	μ
VE_L035_M19	35	1×10^{19}	(P as)	PREM
VE_L100_M19	100	1×10^{19}	1×10^{22}	PREM
VE_L035_M21	35	1×10^{21}	1×10^{22}	PREM
VE_L100_M21	100	1×10^{21}	1×10^{22}	PREM
RIGID	–	1×10^{30}	1×10^{30}	1×10^{20} Pa

Tab. 2: Solid-Earth rheologies used in this study. The controlling parameters are h_L: thickness of lithosphere; η_{UM}: upper mantle viscosity; η_{LM}: lower mantle viscosity and μ: the shear modulus. Note that the values for the RIGID Earth are practically infinite. PREM stands for Preliminary Earth Reference Model (DZIEWONSKI & ANDERSON 1981).

Tab. 2: Rheologien der festen Erde, wie sie in dieser Studie verwendet werden. Die variablen Parameter sind die Mächtigkeit der Lithosphäre h_L, die Viskosität des oberen Mantels η_{UM}, die des unteren Mantels η_{LM}, sowie das elastische Schermodul μ. Man beachte, dass die Werte im Falle der RIGID Erde praktisch unendlich sind. PREM steht für Preliminary Earth Reference Model (DZIEWONSKI & ANDERSON 1981).

Additionally, by applying practically infinite values for the viscosity (1×10^{30} Pa s) and the shear modulus (1×10^{20} Pa), the effects of a rigid (i.e., non-deforming) Earth (labelled as RIGID), which allows only for gravitational feedbacks, are investigated. The labels for viscoelastic rheologies (VE) are made up of sub-labels: L035 and L100 indicating the lithosphere thickness, and M19 and M21, indicating the logarithm of upper mantle viscosity.

The results from the coupled model are compared with simulations featuring the ELRA approximation for solid-Earth dynamics (see Section ELRA). With the elastic structure given by PREM, the flexural rigidity D can be related to the thickness of the lithosphere (LAMBECK & NAKIBOGLU 1980). However, since the viscoelastic layering in the SGVEM implies a full spectrum of relaxation times, the single ELRA relaxation time τ_r cannot be related to the SGVEM viscoelastic structures uniquely (VAN DEN BERG et al. 2008). The combinations of the considered ELRA parameters are listed in Table 3: The values $D = 1\times10^{23}$ N m and $D = 2.5\times10^{24}$ N m include the 35 km lithosphere, while $D = 1\times10^{25}$ N m and $D = 3\times10^{25}$ N m comprise the 100 km lithospheres. For the relaxation time, $\tau_r = 20$ yr and $\tau_r = 500$ yr are chosen for comparison with the low-viscous upper mantle and $\tau_r = 1000$ yr and $\tau_r = 5000$ yr for the high-viscous upper mantle.

ELRA run No	D (N m)		τ_r(yr)	Corresponding VE layering
1	1×10^{23}	(20 km)	20	VE_L035_M19
2	2.5×10^{24}	(54 km)	20	VE_L035_M19
3	1×10^{23}	(20 km)	500	VE_L035_M19
4	2.5×10^{24}	(54 km)	500	VE_L035_M19
5	1×10^{25}	(84 km)	1000	VE_L100_M21
6	3×10^{25}	(119 km)	1000	VE_L100_M21
7	1×10^{25}	(84 km)	5000	VE_L100_M21
8	3×10^{25}	(119 km)	5000	VE_L100_M21

Tab. 3: ELRA parameters: The viscoelastic layering, to which the respective ELRA run is compared, is indicated (Tab. 2). The bracketed values give the lithospheric thickness corresponding to D.

Tab. 3: Parameter des ELRA-Ansatzes: Die viskoelastische Schichtung, dem der entsprechende ELRA-Modelllauf zugeordnet wird, ist angegeben (vgl. Tab. 2).

Forcing

The steady-state ice-sheet and ice-shelf configuration is forced out of its equilibrium with a) rising sea level, b) decreased accumulation rate (in terms of changing SMB), or c) decreased accumulation rate and changed conditions at the base of both, the ice shelf and the grounded ice. The applied forcing scenarios are summarized in Table 4.

If the SGVEM is considered for solid-Earth dynamics, the sea-level forcing is applied by removing a uniform ice layer from the remote continent when handing the global ice thickness field from the ISM to the SGVEM: In the two scenarios S120 and S150, the ice is removed at a constant rate of 0.1 m yr^{-1} equivalent sea-level (ESL) from the remote continent starting at t = 100 yr until the maximum forcing of h^f = 120 m ESL or 150 m ESL, respectively, is reached, coinciding with a respective ice volume $\Delta V_{ice}^f = h^f A_{oc}\, \rho_{oc}/\rho$ (ocean area $A_{oc} = 3.68\times10^8$ km^2). For the ELRA-based simulations, these rates are directly applied as sea-level rise, together with the sea-level rise from the retreating modelled ice sheet (see Section ELRA).

The applied rate of global sea-level rise is approximately twice as large as the highest rates during the last deglaciation (meltwater pulse 1A: 20 m in ~500 yr; WEAVER et al. 2003). This high value, as well as the high amplitudes of more than 120 m ESL is due to the relatively low sensitivity of the ice-sheet model to sea-level rise (see Section DISCUSSION). This should, however, not affect the systematic effects found in the later results.

In the third scenario (labelled as ACCU), a linear decrease in the accumulation rate from 0.2 m/yr to 0.1 m/yr is realised between t = 100 yr and t = 600 yr. The fourth scenario (labelled as BASL) addresses the basal parameters in the ISM. It adopts the ACCU accumulation rate change together with an increased parameter A_{eff} in Equation 1 (sub-shelf melting increases to values of >0.18 m/yr) as well as reduced basal friction at $t = 0$.

Scenario	h^f (m)	ΔV^f_{ice} (km^3)	t_{start}/t_{end} (yr)	$\dot{b}_s$ (m WE/yr)	A_{eff} (m^2)	C (Pa (m/s)$^{1/3}$)
S120	120	-4.8×10^7	100/1300	0.2*	10^{-3}*	1.0×10^7*
S150	150	-5.9×10^7	100/1600	0.2*	10^{-3}*	1.0×10^7*
ACCU	0*	0*	100/600	0.1	10^{-3}*	1.0×10^7*
BASL	0*	0*	100/600	0.1	0.01	0.7×10^7*

Tab. 4: Applied forcing scenarios: The forced equivalent sea-level rise h^f corresponds to the ice volume removed from the remote continent ΔV^f_{ice}. Start and end time refer to the melting pulse from the remote continent (S120, S150) or to the interval for linear decrease of the SMB to the given value (ACCU, BASL). $\dot{b}_s$ is the model domain-wide SMB, A_{eff} is the tuning parameter for basal melting in the shelf regions (Equation 1), and C is the basal friction coefficient. Asterisk-indexed values are unchanged in the respective scenario.

Tab. 4: Verwendete Antriebsszenarien: Der äquivalente Meeresspiegelanstieg h^f entspricht dem Eisvolumen ΔV^f_{ice}, das vom entfernt liegenden Kontinent entnommen wird. Die Zeitpunkte t_{start} und t_{end} beschreiben das Intervall des Schmelzens auf dem entfernt liegenden Kontinent (S120, S150) oder der linearen Abnahme der Oberflächenmassenbilanz auf den angegeben Werten (ACCU, BASL). $\dot{b}_s$: Im gesamten Modellbereich angewandte Oberflächenmassenbilanz, A_{eff}: Kontrollparameter für basales Schmelzen im Schelfeis (Gleichung 1). C: Koeffizient für die basale Reibung. Werte mit Sternchen versehen sind in dem entsprechenden Szenario unverändert.

RESULTS

General findings

In all scenarios with non-rigid solid-Earth modelled by either ELRA or the SGVEM, the forced GL retreat decelerates and eventually ceases. Figure 2 shows the initial geometry and the final geometry for the VE_L035_M19 and VE_L100_M21 simulations under the S120 forcing along the cross section coinciding with the *y*-axis of the ISM domain (Fig. 1). Here, a first effect of the viscoelastic layering of the solid-Earth on the ice dynamics becomes visible: A more localised and faster uplift of the solid Earth (VE_L035_M19 – Fig. 2B) leads to less GL retreat than a long-wave and slower response (VE_L100_M21 – Fig. 2C). The backward slopes at the GL, however, at least partially remain. This is not surprising as GL retreat is treated in a three-dimensional set-up here. Consequently, GL stability is not only determined by the bedrock gradient, but also by the stress field in the ice body (GUDMUNDSSON et al. 2012, GUDMUNDSSON 2013).

Figure 3 shows the GL retreat along the central cross section over 15 or 20 kyr, respectively, for the four applied forcing scenarios and the five SGVEM Earth structures. The stepwise GL retreat, as it can be seen in the time series, is a feature of the numerical approach to the GL migration. The GL – and thus the whole ice sheet – on the RIGID Earth is not yet in steady state at the end of the illustrated time spans in all four forcing scenarios. On a viscoelastically adjusting Earth, the GL retreat has stopped before $t = 7$ kyr (S120, S150), or $t = 10$ kyr (ACCU) and $t = 15$ kyr (BASL). The exact time depends on the viscoelastic layering and the forcing strength. At this stage, only maximum GL retreat during each experiment is considered. The respective ice/Earth configuration is not necessarily in a steady state: Below, the possibilities of GL re-advance after reaching the maximum GL retreat distance will be discussed.

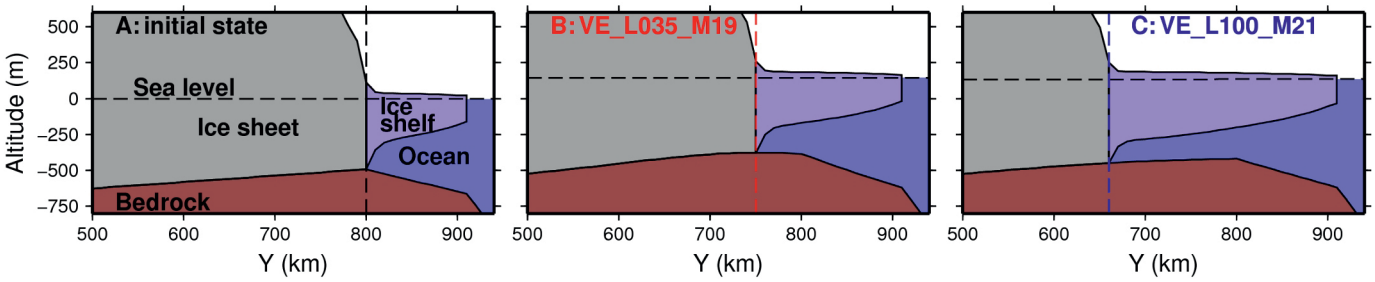

Fig. 2: Cross sections through the ice sheet. A: at time $t = 0$; B: after 8000 yr for VE_L035_M19 simulation; C: for VE_L100_M21 simulation at $x = 0$ for the S120 forcing. The grounding line (GL) positions correspond to the vertical dashed lines.

Abb. 2: Querschnitte ($x = 0$) durch den Eisschild zum Zeitpunkt $t = 0$ (A) und nach 8000 Jahren im Falle der VE_L035_M19-Simulation (B) und der VE_L100_M21-Simulation (C) und dem S120-Szenario. Die Positionen der Aufsetzlinie (GL) entsprechen den senkrechten, gestrichelten Linien.

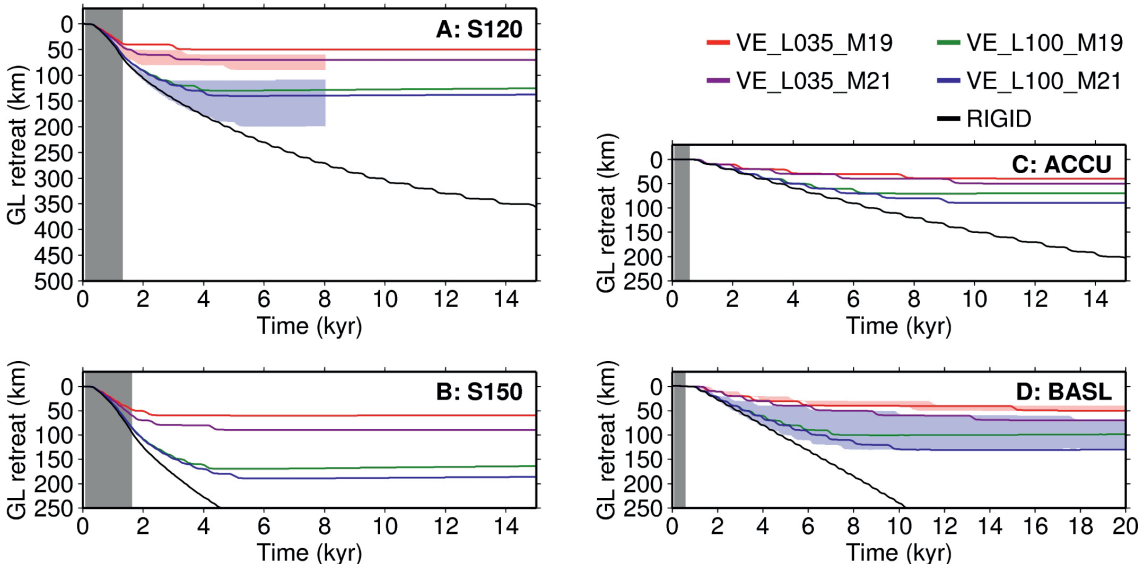

Fig. 3: Time series of GL retreat for the A: S120, B: S150, C: ACCU, and D: BASL forcing scenarios. The GL retreat refers to the $x = 0$ cross section (Fig. 1). The grey areas mark the periods of gradual melting on the remote continent and thus the forced sea-level rise (S120, S150), or the time interval of decreasing SMB (ACCU, BASL). The red shaded areas in A and D indicate the results spanned by the applied ELRA parameters corresponding to the VE_L035_M19 layering (Tab. 3). The blue shaded area shows the respective comparative ELRA results for the VE_L100_M21 layering. Note that the time series in D show data until $t = 20$ kyr, whereas it is only 15 kyr in A through C.

Abb. 3: Zeitreihen des Rückzugs der Aufsetzlinie im Falle der Antriebsszenarien A: S120, B: S150, C: ACCU und D: BASL. Der Rückzug bezieht sich auf den $x = 0$ Querschnitt (Abb. 1). Die grauen Bereiche bezeichnen die Intervalle des allmählichen Abschmelzens auf dem entfernt liegenden Kontinent (entspricht dem angetriebenen Meeresspiegelanstieg, S120, S150) oder das Intervall, in welchem die Oberflächenmassenbilanz abnimmt (ACCU, BASL). Die roten Bereiche in A und D umfassen die zu VE_L035_M19 gehörigen ELRA-Ergebnisse (Tab. 3). Die blauen Bereiche zeigen die entsprechenden zu VE_L100_M21 gehörigen ELRA-Ergebnisse. Man beachte, dass die Zeitreihen in D über 20.000 Jahre gehen, während es im Fall von A, B und C nur 15.000 Jahre sind.

There are notable systematic differences between the viscoelastic settings: The ice sheet in the case of a fast adjusting, low-viscous upper mantle (VE_L035_M19, VE_L100_M19) is less sensitive in terms of final GL position along the y-axis to the GL retreat forcing than in the case of the high-viscous upper mantle (VE_L035_M21, VE_L100_M21). Additionally, in both of these subgroups, the thinner lithosphere (L035) leads to less GL response to the forcing. The maximum retreat distances along the cross section are listed in Table 5. It is also visible that simulations with a low-viscous upper mantle are less sensitive to an increase in forcing: the maximum retreat positions under the S120 and S150 forcings differ only by 10 km and 20 km, while the higher upper mantle viscosity leads to respective differences of 40 km and 50 km.

Scenario	VE_L035_M19	VE_L100_M19	VE_L035_M21	VE_L100_M21
S120	50	70	130	140
S150	60	90	170	190
ACCU	40	50	70	90
BASL	50	70	100	130

Tab. 5: Maximum distances of grounding line (GL) retreat in km along the $x = 0$ cross section as inferred from Fig. 3. The possible re-advance as discussed in Fig. 6 is not considered here.

Tab. 5: Maximale Strecken des Aufsetzlinienrückzuges (GL) entlang des $x = 0$ Querschnittes (in km), wie sie aus Abb. 3 abgelesen werden können. Ein möglicher Wiedervorstoß, wie in Abb. 6 gezeigt, ist hier unberücksichtigt.

Comparison with ELRA under the S120 forcing

Figure 3A shows the results of the ELRA simulations under the S120 forcing with different choices for the flexural rigidity D and the relaxation time τ_r (red and blue shading). Overall, the ELRA simulations are similar to those with the real viscoelastic coupling in terms of the effect on the GL retreat: the faster and more local the solid-Earth can adjust to the unloading by a GL retreat, the less sensitive the ice sheet responds to the forcing.

Here, however, the ELRA approximation reveals shortcomings by a considerably higher sensitivity to the applied forcing: While the VE_L100_M21 results lie in the range of the respective ELRA results and consistency is hence given in terms of GL retreat, the comparison of VE_L035_M19 to the respective ELRA results indicates that the ice sheet with the ELRA response is more sensitive to the forcing even in the case of extremely low values for the relaxation time τ_r and flexural rigidity D. The ELRA results in this parameter range seem more appropriate for the VE_L100_M19 with its thicker lithosphere than for the VE_L035_M19 case. This is due to the higher sea level in the ELRA runs as a consequence of not considering the sea-level drop due to the ice-sheet retreat.

This higher sensitivity to sea-level rise in the ELRA approximation can be found more indirectly in the comparison of the "well-fitted" VE_L100_M21 results with those from ELRA: Figure 4 shows the RSL at the GL as it retreats for VE_L100_M21 and two respective ELRA simulations. The time markers along the graphs show that the RSL falls faster in the ELRA simulations in general and so should provide earlier stability. The coverage of the VE_L100_M21 results by the ELRA in the case of the S120 forcing results must then be due to the overestimation of sea-level rise.

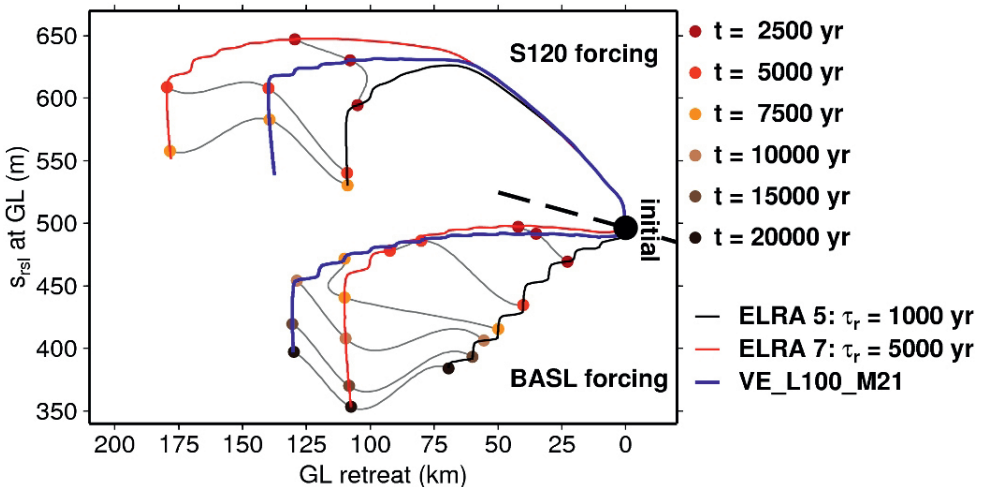

Fig. 4: Relation between RSL s_{rsl} at the GL and GL position along the central cross section in the S120 and BASL forcing scenarios for the VE_L 100_M21 Earth and two of the corresponding ELRA parameterisations (No. 5 and 7; Tab. 3). All simulations start from the same initial state; consequently, all graphs are to be read from the black marker at approximately (0 km, 500 m). At given times (colour-coded dots), the ELRA and SGVEM graphs are connected by grey lines. The black dashed line separates the S120 and the BASL results.

Abb. 4: Zusammenhang zwischen relativem Meeresspiegel s_{rsl} an der Aufsetzlinie (GL) und Position der Aufsetzlinie (GL) entlang des Querschnittes bei $x = 0$ im Falle der Antriebsszenarien S120 und BASL und der VE_L100_M21-Erdparametrisierung, sowie für zwei der zugehörigen ELRA-Parametrisierungen (Nr. 5 und 7, vgl. Tab. 3). Alle Simulationen beginnen bei demselben initialen Zustand; entsprechend sollten alle abgebildeten Graphen von dem schwarzen Marker bei ungefähr (0 km, 500 m) aus gelesen werden. Zu angegebenen Zeitpunkten, markiert durch die farbigen Punkte, sind die zu ELRA gehörigen Graphen und die zum vollwertigen Erdmodell gehörigen Graphen durch graue Linien verbunden. Die schwarze gestrichelte Linie trennt die S120 und die BASL Ergebnisse.

Comparison with ELRA under the BASL forcing

In the scenarios without externally forced sea-level rise, the BASL scenario shall be evaluated exemplarily in terms of ELRA and SGVEM differences. The main difference to the sea-level forced scenarios is that the forcing does not only affect the ice sheet directly at the GL, but that the whole ice sheet shrinks and, due to the changes in the basal parameters, changes its geometry. The ice flow is accelerated by the decrease in basal friction, such that more ice is transported towards the margins. The overall unloading of the continent due to the shrinkage leads to considerable uplift that stabilises the GL to some extent even before it starts to retreat.

The VE_L035_M19 und the respective ELRA simulations

(red shading) are consistent in this scenario (Fig. 3d) in terms of the inclusion of the VE_L035_M19 results by the ELRA results. Due to the small increase in sea level from melting of the ice sheet, which results in less than 4 m eustatic sea-level rise for the ELRA runs No 1-4 (see Tab. 3 for the numbering), the above drawback concerning non-consistent sea-level rise is of minor importance.

The same comparison for the VE_L100_M21 simulation and the respective ELRA runs (No 5-8), however, shows a clear preference towards τ_r = 5000 yr: While τ_r = 1000 yr to 5000 yr reproduce the VE_L100_M21 results under the S120 forcing, different τ_r parameters need to be chosen to encompass the combination of VE_L100_M21 layering and BASL forcing. As for the S120 forcing, the respective graphs in Figure 4 show a faster RSL fall at the GL in the ELRA simulations. In the BASL scenario, this relatively fast Earth response is not compensated by an overestimated sea-level rise as in S120 so that the slower relaxation of the solid-Earth effectively yields more GL retreat for the VE_L100_M21 simulation.

Relation between ice dynamical and solid-Earth time scales

A feature of the simulations with a low-viscous upper mantle is the significantly increasing time span between two discrete GL steps in the model. These are partially of the order of several thousand years in the presented scenarios, whereas the high-viscous upper mantle runs feature a modest increase of the time intervals before the next GL step. As already mentioned above, the stepwise character is a numerical feature, but the long time spans in the case of low upper mantle viscosity still contains a physical message, as will be discussed here.

The BASL scenario serves as a prominent example for comparing the time scales of solid-Earth relaxation and ice-flow adjustment to the changed conditions for the thin lithosphere runs VE_L035_M19 and VE_L035_M21 and for the RIGID Earth. Figure 5 shows the time series of RSL at the GL (again along the central cross section) and GL flux integrated along the whole GL, confining the ice shelf. In order to not focus on numerical aspects of GL migration, the smoothened time series (solid, thick lines; obtained as running mean) are considered. Three issues concerning the phenomena shown in Figure 5 can be highlighted:

(1) There is a GIA-induced fall of RSL at the GL in the viscoelastic runs: Following the GL retreat, there is unloading around the GL and thus bedrock uplift and sea-level fall. This is not the case for the RIGID Earth, where a steady increase of RSL occurs due to the backward sloping design of the bedrock geometry until flatter areas are reached ($t \approx$ 16 kyr).
(2) The time intervals between two GL steps are equal over the whole time span for the RIGID run (distance between neighbouring vertical black lines in Figure 5), indicating an almost constant GL retreat velocity of ~25 m/yr. In the viscoelastic runs, the GL velocity slows down due to the partial adjustment to the unloading. This transition is modest in the VE_L035_M21 run, whereas the time to cover the last 10 km distance in the VE_L035_M19 run is longer than 9 kyr, meaning that the GL velocity is only slightly above zero over this time span.
(3) The integrated GL flux is much higher in the RIGID simulation as a constantly high amount of ice is transported from the inland to the shelf. In the case of a viscoelastically adjusting Earth, the GL flux decreases as the ice dynamics approaches a steady state. After the GL retreat is decelerated such that there is no more GL migration on grid scale, the GL flux decays towards the limit of ~34 km^3/yr. In the case of the VE_L035_M21 layering, the respective time scale is much smaller than the time scale of RSL relaxation (high-viscous upper mantle). In the case of the VE_L035_M19 layering, the respective time scales appear to be of similar magnitude.

The slow adjustment of RSL in the case of a high-viscous upper mantle has further implications on the GL migration. Figure 6 shows time series of GL retreat along the central cross section for the S150 scenario, extending the time span from 20 kyr shown in Figure 3B to 50 kyr. Here, a gradual GL re-advance of the GL on the VE_L035_M21 Earth starts after the maximum distance is reached at $t \approx$ 5 kyr. After approximately 19 kyr, the GL re-advance reaches the grid scale and ends up at a final distance of 113 km away from the initial position and 57 km from the maximum retreat position. This prominent re-advance is, however, a feature of the deformational response of the thin lithosphere: A comparable evolution cannot be found for the VE_L100_M21 simulation before t = 50 kyr although a sub-grid scale re-advance occurs.

DISCUSSION

Our general finding, that viscoelastic deformation can decelerate and stop GL retreat, is in accordance with Gomez et al. (2012). The actual evolution through time depends on the solid-Earth parameters, namely thickness of the lithosphere and mantle viscosity. The first one determines how localised the solid-Earth responds to the unloading caused by an ice mass loss. As a more localised response leads to a more effective compensation of the former backward slopes, GL stability is reached at sites closer to the initial GL location. Mantle viscosity, in contrast, affects the time scale on which the solid-Earth reacts to the change in the loading: The fast response of a low-viscous upper mantle also leads to earlier GL stability than in case of the slower response of a high-viscous mantle and so to less GL retreat and ice mass loss.

In the studied situation, the mantle viscosity and the related time scales of solid-Earth response have the dominant impact on maximum GL retreat (Tab. 5) compared to lithosphere thickness. One should, however, state that the grounded ice flow is rather slow in this scenario compared to present-day Antarctic ice streams, which feed the surrounding shelf areas (e.g., ~500 m/yr in the catchment area of the Ross Ice Shelf (Thomas et al. 2013) vs. less than 150 m/yr here). Compared to that, the ice flow in this scenario is potentially less controlled by the underlying bedrock topography.

The initial magnitude of the backward slope also affects the time to reach stability. An ice sheet on a slope of different steepness might then also be more sensitive to lithospheric thickness as it is the case in this scenario. The possibility of GL re-advance yields a greater importance for the lithosphere thickness in later parts of the system's evolution in time.

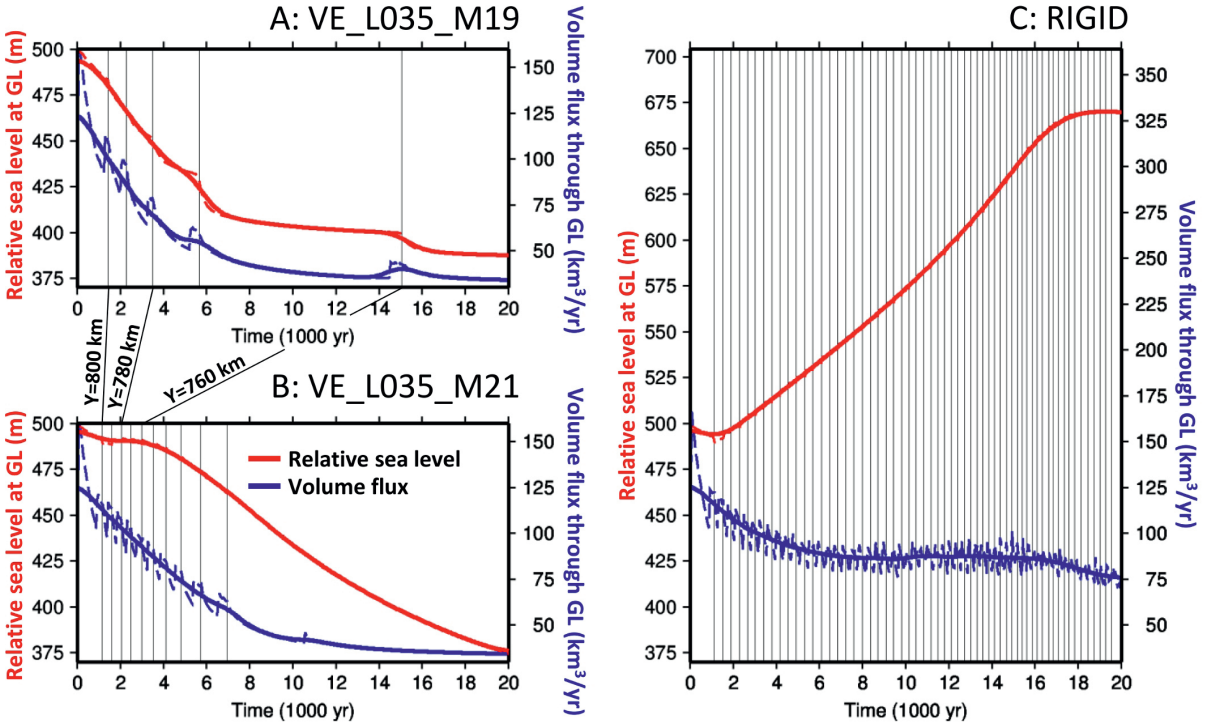

Fig. 5: Time series of RSL at the GL (red; left ordinate) and GL flux (blue; right ordinate); A: for the BASL scenario on the VE_L035_M19 Earth; B: on the VE_L035_M21 Earth and C: on the RIGID Earth. Each black vertical line indicates when the GL passes one of the *y*-grid nodes at $x = 0$. The GL flux is the integrated flux from the inland ice into the ice-shelf area. The GL retreat is considered along the central cross section ($x = 0$). The dashed coloured lines show the originally modelled data; the solid thick lines are obtained from these by running mean application and, hence, are less disturbed by numerical effects of the discrete GL retreat.

Abb. 5: Zeitreihen des relativen Meeresspiegels an der Aufsetzlinie (GL; rot, linke Ordinate) und Eisfluss über die Aufsetzlinie (GL; blau, rechte Ordinate) im Falle des BASL-Szenarios A: auf der VE_L035_M19-Erde, B: auf der VE_L035_M21-Erde und C: auf der RIGID-Erde. Jede senkrechte schwarze, gestrichelte Linie zeigt an, dass die Aufsetzlinie einen weiteren diskreten Punkt des *y*-Gitters entlang des Querschnittes bei $x = 0$ passiert. Der Fluss über die Aufsetzlinie ist integriert über die gesamte Grenzfläche zwischen Eisschild und Schelfeis. Die gestrichelten farbigen Linien zeigen die ursprünglichen Ergebnisse an; die entsprechenden durchgezogenen Linien sind durch Glättung (gleitender Mittelwert) erhalten und sind daher weniger durch den numerischen Effekt des diskreten Rückzuges beeinträchtigt.

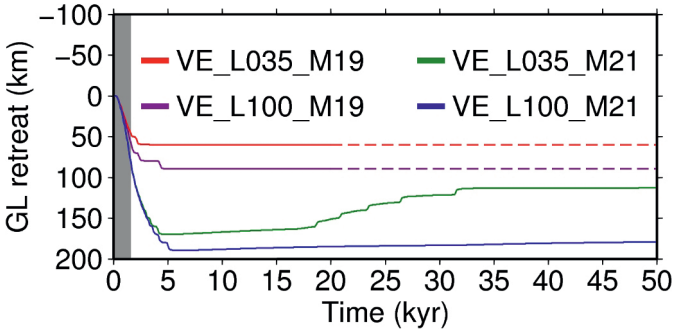

Fig. 6: Time series of grounding line (GL) retreat along the central cross section for the S150 scenario for 50 kyr (Fig. 3B: 15 kyr). The dashed parts in the VE_L035_M19 and VE_L100_M19 time series are extrapolated.

Abb. 6: Zeitreihen des Rückzuges der Aufsetzlinie (GL) entlang des Querschnittes bei $x = 0$ im Falle des Antriebsszenarios S150 über 50.000 Jahre hinweg (vgl. Abb. 3B: 15.000 Jahre). Die gestrichelten Passagen in den Zeitreihen der Erdparametrisierungen VE_L035_M19 und VE_L100_M19 sind extrapoliert.

The common method to account for a coupling between ice and solid-Earth dynamics, the ELRA method, shows similar behaviour as the ISM-SGVEM simulations, but has a major drawback when it comes to sea-level implications. The SLE is not solved within the ELRA approximation. The only possible way of accounting for sea-level rise or fall on glacial-interglacial time scales is to account for the eustatic sealevel. But this simplification overestimates (underestimates) the local sea-level in the ice sheet's vicinity during deglaciation (glaciation), because the gravitational attraction of the oceans by the ice mass is ignored. Hence, the ice sheet's response to sealevel change is amplified. The overestimated sea level can be compensated by an adequate choice of ELRA parameters (faster and more localized adjustment), from which in turn the physical meaning of the ELRA parameters τ_r and D would suffer. The adjustment of the ELRA parameters and the assessment against SGVEM simulations is an important issue even without the requirement of modelling interactions between ice sheets and sea level (VAN DEN BERG et al. 2008, KONRAD et al. 2014). The comparison of results from the VE_L035_M19 and VE_L100_M21 simulations to results from respective ELRA simulations shows that the a priori relaxation time in ELRA has to be chosen shorter than the related relaxation spectrum of a SGVEM in order to adequately model GL retreat in a sea-level rise scenario in general.

The relation between the time scales of solid-Earth relaxation and ice-flow adjustment is also very important for the retreat characteristics and potential re-advance of the GL. A slowly adjusting solid-Earth stabilises the disintegrating ice sheet gradually (VE_L035_M21 graphs in Fig. 5). Depending on the GL retreat velocity and on the delay of the solid-Earth response, the GL can even overshoot the later steady-state position and – after stopping further down-slope – re-advance

when the delayed fall of RSL creates the necessary conditions (Fig. 6). This, however, also depends on the lithosphere thickness: The thick lithosphere in the VE_L100_M21 simulation and the related long-wavelength pattern of RSL fall prevent the GL from re-advancing.

A fast adjusting solid-Earth interacts with the ice sheet in a more complex way. Depending on the ice-rheological parameters and the stress field in the ice, it takes the ice dynamics a certain time to adjust to new boundary conditions. In the case shown in Figure 5, these new conditions comprise the new SMB and the changed basal conditions (BASL), as well as the constantly adjusting ice-sheet geometry due to GL retreat. If the Earth beneath the ice sheet adjusts faster than or with similar time scales as the ice flow adjusts to the new conditions, the approach towards the final steady state becomes very slow. This manifests numerically in the long time spans between two grid-scale GL retreat events.

A general feature of the presented results is the insensitivity of the ice sheet to the applied forcing: The GL retreats over 190 km at most – under the most unrealistic condition of a 150 m rise of global mean sea level within 1500 yr (Tab. 5). Although this might be attributed to the specific set-up, it points at the inert representation of the GL, if this is not treated beyond the application of the SIA on the one and SSA on the other side of the GL and the floating criterion to separate these two areas (Pattyn et al. 2013). This drawback hinders clearer conclusions with respect to the relation of time scales of the ice and the Earth.

CONCLUSIONS

The feedback of RSL on GL migration has been treated extensively in this study. In the simplified situation considered here, the differences in the Earth representation – be it due to application of different approaches (ELRA *versus* SGVEM) or due to different choices for the viscoelastic parameters – lead to systematic differences in the ice sheet's evolution. In particular, the fast adjustment of an Earth with low mantle viscosities, as well as the high amplitudes of deformation of a relatively thin lithosphere yield a stronger negative feedback on GL migration than higher mantle viscosities and thicker lithospheric layers on glacial time scales. This indicates that a thorough consideration of the determining Earth parameters is necessary when studying ice dynamics, e.g., through past glacial cycles.

The simplified Earth dynamics of the ELRA approximation yield an essential conceptual drawback when it comes to the feedback of ice sheets with the solid Earth via the GL positioning and sealevel. Firstly, ELRA does not allow treating sea level gravitationally consistently, which leads to a possible overestimation of the related effects. Secondly, the dependence of the relaxation time on the load dimension and the viscoelastic stratification can become important, when it comes to GL migration in a MISI scenario; the usage of a single *a priori* relaxation time in ELRA, despite the wavelength-dependent relaxation spectrum associated with a more realistic Earth model description (e.g., Spada et al. 2011), introduces a bias in the evolution of the grounded ice, particularly if the ELRA parameters are not carefully tuned. Already in the simplified ice-sheet set-up in this study, it is difficult to define ELRA parameters, such that the effects from overestimated local RSL, inaccurate surface deformation and mantle relaxation are minimized. The problem becomes even more important for the simulation of an ice-sheet history through glacial cycles, as the ice sheet's response is sensitive to both, sea-level variations and atmospheric conditions. To avoid these drawbacks, a coupled model system such as the presented or that by Gomez et al. (2012, 2013) or de Boer et al. (2014) should be used, as it self-consistently accounts for sea-level variations and surface deformations.

ACKNOWLEDGMENTS

The authors wish to thank Heinz Miller for his thorough review and helpful suggestions and the editor Dieter Fütterer for handling the manuscript. HK is funded by the German Research Foundation (DFG) through grant SA 1734/6-1. This study has partially been funded in the framework of the DFG priority program SPP1257 "Mass transport and mass distribution in the Earth system" through grant SA 1734/2-2. IS acknowledges funding through DFG grant SA 1734/4-1. ZM acknowledges support from the Science Foundation of Ireland through the research program 11/RFP.1/GEO/3309. The study is also a contribution to the Helmholtz Climate Initiative REKLIM, a joint research project of the Helmholtz Association of German Research Centres (HGF).

References

Abramowitz M. & Stegun, I.A. (eds) (1964): Handbook of Mathematical Functions with Formulas, Graphs, and Mathematical Tables.- Dover 1-1046.

Beckmann, A. & Goosse, H. (2003): A parameterization of ice shelf-ocean interaction for climate models.- Ocean Model. 5(2): 157-170, doi: 10.1016/S1463-5003(02)00019-7.

Bindschadler, R.A. & 26 co-authors (2013): Ice-sheet model sensitivities to environmental forcing and their use in projecting future sea level (the SeaRISE project).- J. Glaciol. 59 (214): 195-224, doi: 10.3189/2013JoG12J125.

Brotchie, J.F. & Silvester, R. (1969): On crustal flexure.- J. Geophys. Res. 74: 5240-5252, doi: 10.1029/JB074i022p05240.

Cuffey, K.M. & Paterson, W.S.B. (2010): The Physics of Glaciers.- Elsevier Science, 4th edition, ISBN 9780080919126, 1-704.

de Boer, B., Stocchi, P. & van de Wal, R.S.W. (2014): A fully coupled 3-D ice-sheet – sea-level model: algorithm and applications.- Geosci. Model Dev. Discuss. 7: 3505-3544, doi: 10.5194/gmdd-7-3505-2014.

Dziewonski, A.M. & Anderson, D.L. (1981): Preliminary reference Earth model.- Phys. Earth Planet. Inter. 25: 297-356, doi: 10.1016/0031-9201(81)90046-7.

Farrell, W. & Clark, J. (1976): On postglacial sea level.- Geophys. J. Astr. Soc. 46: 647-667, doi: 10.1111/j.1365-246X.1976.tb01252.x.

Foldvik, A. & Kvinge, T. (1974): Conditional instability of sea water at the freezing point.- Deep-Sea Res. 21: 169-174, doi: 10.1016/0011-7471(74)90056-4.

Gomez, N., Pollard, D., Mitrovica, J.X., Huybers, P. & Clark, P.U. (2012): Evolution of a coupled marine ice sheet–sea level model.- J. Geophys. Res. 117: F01013, doi: 10.1029/2011JF002128.

Gomez, N., Pollard, D. & Mitrovica, J.X. (2013): A 3-D coupled ice sheet – sea level model applied to Antarctica through the last 40 ky.- Earth Planet. Sci. Lett. 384: 88-99, doi: 10.1016/j.epsl.2013.09.042.

Greve, R., Saito, F. & Abe-Ouchi, A. (2011): Initial results of the SeaRISE numerical experiments with the models SICOPOLIS and IcIES for the Greenland Ice Sheet.- Ann. Glaciol. 52(58): 23-30, doi: 10.3189/172756411797252068.

Gudmundsson, G.H., Krug, J., Durand, G., Favier, L. & Gagliardini, O. (2012): The stability of grounding lines on retrograde slopes.- The Cryosphere 6: 1497-1505, doi: 10.5194/tc-6-1497-2012.

Gudmundsson, G.H. (2013): Ice-shelf buttressing and the stability of marine ice sheets.- The Cryosphere 7: 647-655, doi: 10.5194/tc-7-647-2013.

Hagedoorn, J.M., Wolf, D. & Martinec, Z. (2007): An estimate of global mean sea-level rise inferred from tide-gauge measurements using glacial-iso-

static models consistent with the relative sea-level record.- Pure Appl. Geophys. 164: 791-818, doi: 10.1007/s00024-007-0186-7.

Haskell, N.A. (1935): The motion of a viscous fluid under a surface load.- J. Appl. Phys. 6: 265-269, doi: 10.1063/1.1745329.

Huybrechts, P. (1993): Glaciological modelling of the late Cenozoic East Antarctic Ice Sheet: stability or dynamism?- Geogr. Ann. Phys. Geogr. 75: 221-238, URL http://www.jstor.org/stable/521202.

Huybrechts, P., Goelzer, H., Janssens, I., Driesschaert, E., Fichefet, T., Goosse, H. & Loutre M.-F. (2011): Response of the Greenland and Antarctic Ice Sheets to multi-millennial greenhouse warming in the Earth system model of intermediate complexity LOVECLIM.- Surv. Geophys., 32(4-5): 397-416, doi: 10.1007/s10712-011-9131-5.

Konrad, H., Thoma, M., Sasgen, I., Klemann, V., Barbi, D., Grosfeld, K. & Martinec, Z. (2014): The deformational response of a viscoelastic solid earth model coupled to a thermomechanical ice sheet model.- Surv. Geophys. 35: 1441-1458, doi: 10.1007/s10712-013-9257-8.

Lambeck, K. & Nakiboglu, S.M. (1980): Seamount loading and stress in the ocean lithosphere.- J. Geophys. Res. 85B: 6403-6418, doi: 10.1029/JB085iB11p06403.

Le Meur, E. & Huybrechts, P. (1996): A comparison of different ways of dealing with isostasy: examples from modeling the Antarctic ice sheet during the last glacial cycle.- Ann. Glaciol. 23: 309-317.

Maris, M.N.A., de Boer, B., Ligtenberg, S.R.M., Crucifix, M., van de Berg, W.J. & Oerlemans, J. (2014): Modelling the evolution of the Antarctic Ice Sheet since the last interglacial.- The Cryosphere 8: 1347-1360, doi: 10.5194/tc-8-1347-2014.

Martinec, Z. (2000): Spectral-finite element approach to three-dimensional viscoelastic relaxation in a spherical Earth.- Geophys. J. Int. 142: 117-141, doi: 10.1046/j.1365-246x.2000.00138.x.

Mitrovica, J.X. & Milne, G.A. (2003): On post-glacial sea level: I. General theory.- Geophys. J. Int. 154: 253-267, doi: 10.1046/j.1365-246X.2003.01942.x.

Mitrovica, J.X., Tamisiea, M.E., Davis, J.L. & Milne, G.A. (2001): Recent mass balance of polar ice sheets inferred from patterns of global sea-level change.- Nature 409: 1026-1029, doi: 10.1038/35059054.

Oerlemans, J. (1980): Model experiments on the 100,000-yr glacial cycle.- Nature 287: 430-432, doi: 10.1038/287430a0.

Pattyn, F. & 27 co-authors (2013): Grounding-line migration in plan-view marine ice-sheet models: results of the ice/sea MISMIP3d intercomparion.- J. Glaciol. 59: 410-422, doi: 10.3189/2013JoG12J129.

Peltier, W.R. (1974): The impulse response of a Maxwell Earth.- Rev. Geophys. 12: 649-669, doi: 10.1029/RG012i004p00649.

Pollard, D. & DeConto, R.M. (2009): Modelling West Antarctic Ice Sheet growth and collapse through the past five million years.- Nature 458: 329-332, doi: 10.1038/nature07809.

Pollard, D. & DeConto, R.M. (2012): Description of a hybrid ice sheet-shelf model, and application to Antarctica.- Geosci. Model Dev. 5: 1273-1295, doi: 10.5194/gmd-5-1273-2012.

Schoof, C. (2007): Ice sheet grounding line dynamics: Steady states, stability, and hysteresis.- J. Geophys. Res. 112:, doi: 10.1029/2006JF000664.

Spada, G., Barletta, V.R., Klemann, V., Riva, R.E.M., Martinec, Z., Gasperini, P., Lund, B., Wolf, D., Vermeersen, L.L.A. & King, M.A. (2011): A benchmark study for glacial isostatic adjustment codes.- Geophys. J. Int. 185: 106-132, doi: 10.1111/j.1365-246X.2011.04952.x.

Spada, G., Bamber, J.L. & Hurkmans, R.T.W.L. (2013): The gravitationally consistent sea-level fingerprint of future terrestrial ice loss.- Geophys. Res. Lett. 40: 482-486, doi: 10.1029/2012GL053000.

Thoma, M., Grosfeld, K., Barbi, D., Determann, J., Goeller, S., Mayer, C. & Pattyn, F. (2014): RIMBAY – a multi-approximation 3D ice-dynamics model for comprehensive applications: model description and examples.- Geosci. Model Dev. 7: 1-21, doi: 10.5194/gmd-7-1-2014.

Thomas, R., Scheuchl, B., Frederick, E., Harpold, R., Martin, C. & Rignot, E. (2013): Continued slowing of the Ross Ice Shelf and thickening of West Antarctic Ice streams.- J. Glaciol. 59: 838-844, doi: 10.3189/2013JoG12J122.

Thomas, R.H. & Bentley, C.R. (1978): A model for Holocene retreat of the west Antarctic Ice Sheet.- Quat. Res. 10: 150-170, doi: 10.1016/0033-5894(78)90098-4.

van den Berg, J., van de Wal, R.S.W., Milne, G.A. & Oerlemans J. (2008): Effect of isostasy on dynamical ice sheet modeling: A case study for Eurasia.- J. Geophys. Res. 113: B05412, doi:10.1029/2007JB004994.

Weaver, A.J., Saenko, O.A., Clark, P.U. & Mitrovica, J.X. (2003): Meltwater pulse 1A from Antarctica as a trigger of the Bølling-Allerød warm interval.- Science 299: 1709-1713, doi: 10.1126/science.1081002.

Weertman, J. (1957): On the sliding of glaciers.- J. Glaciol. 3: 33-38.

Wessel, P. & Smith, W.H.F. (1991): Free software helps map and display data.- Eos Trans. AGU 72: 441, doi: 10.1029/90EO00319.